Continuous-Aperture OAM Communication Systems: An Electromagnetic Information Theory Perspective

Young-Seok Lee, *Student Member, IEEE*, Young Dam Kim, and Bang Chul Jung, *Senior Member, IEEE*

***Abstract*—We present a novel *continuous-aperture* orbital angular momentum (CAP-OAM) communication system, which can be regarded as an asymptotic generalization of existing (discrete) uniform circular array-based OAM (UCA-OAM) systems. We first derive the current distribution that generates OAM mode in the CAP-OAM transmitter and specify the resulting radiated electric field. We characterize a closed-form equivalent discrete wireless channel model of the CAP-OAM system, which rigorously captures the effect of various system parameters, including path loss, carrier frequency, antenna aperture size, transmission distance, polarization interferences, etc. We also define the effective degrees of freedom (DoF) and mathematically analyze the achievable rate of CAP-OAM systems. Through computer simulations, we confirm that the CAP-OAM system significantly outperforms the classical UCA-OAM system in terms of achievable rates and effective DoF. To the best of our knowledge, CAP-OAM communication systems have not been investigated from the perspective of electromagnetic information theory.**

***Index Terms*—6G, orbital angular momentum (OAM), continuous-aperture MIMO (CAP-MIMO), electromagnetic information theory, equivalent channel model, achievable rate.**

I. Introduction

RECENTLY, *continuous-aperture* MIMO (CAP-MIMO), also known as *holographic* MIMO where the transceiver consists of *spatially-continuous* antennas such as a lens-based array, meta-surface antennas, large intelligent surfaces (LISs), etc, has been actively investigated to enhance the communication performance of LoS-MIMO systems [1], [2], [3], [4]. Unlike the classical MIMO systems with discrete antennas, CAP-MIMO systems assume that arbitrary current distributions can be generated with continuous aperture antennas at both transmitter and receiver and adopt electromagnetic theory to model the wireless channel between them. Thus, *electromagnetic information theory* (EIT) has been developed to theoretically analyze ultimate communication performance and derive the fundamental design principles of CAP-MIMO systems [4], [5].

On the other hand, orbital angular momentum (OAM)-based communication has attracted much attention as a promising solution that achieves high spatial multiplexing gain even in a LoS-MIMO environment over high-frequency bands. OAM can be generated with spatially continuous antenna systems such as spiral phase plate (SPP), but SPP is not appropriate to generate multiple modes simultaneously [6]. To address this, an OAM-based communication system with discrete uniform circular array (UCA) antennas was proposed, and a multi-mode OAM transmission technique with UCA was investigated in [7]. Thanks to the development of metamaterial technology, an OAM-based communication system using a transmissive metasurface for the terahertz band has been proposed in [8]. Moreover, the OAM techniques have been recognized as promising solutions for wireless backhaul networks or satellite-to-vehicle communication systems [9], [10]. In [11], the angle of arrival estimation and transceiver alignment of OAM beams for wireless backhaul were studied. In [12], a holographic OAM system was presented where both transmitter and receiver have spatially continuous antennas again, identifying the relationship between OAM and communication modes when considering LISs in the transceiver. To the best of our knowledge, continuous aperture-based OAM (CAP-OAM) systems from an EIT perspective have not been investigated in the literature.[1]

In this letter, we present a novel CAP-OAM communication architecture with a one-dimensional metamaterial-based continuous aperture transceiver to generate arbitrary current distributions at both transmitter and receiver for OAM mode-division multiplexing (MDM) that conveys information via multiple orthogonal OAM modes [8], [14]. We also rigorously analyze the CAP-OAM communication system based on electromagnetic (EM) wave theory.

II. System Model of CAP-OAM

As illustrated in Fig. 1, we consider an origin-centered continuous ring antenna-based OAM transmitter with a radius of ρ on the x–y plane and a continuous ring antenna-based OAM receiver with a radius of η separated by a transmission distance D along the z-axis. It is assumed that the OAM transmitter and receiver are perfectly aligned as in many relevant studies [3], [4], [12] and neither external source nor multipath signal is considered to focus on the fundamental analysis of CAP-OAM systems. A source point $\mathbf{s}(\in \mathbb{R}^3)$ on the

Received 7 September 2024; revised 4 November 2024; accepted 7 November 2024. Date of publication 18 December 2024; date of current version 10 March 2025. This work was supported in part by the National Research Foundation of Korea (NRF) Grant funded by the Korean Government (MSIT), Research on Interdisciplinary Wireless Communication Technology for Intra-Tube High-Speed Mobility under Grant RS-2024-00420013, and in part by the Institute of Information and Communications Technology Planning and Evaluation (IITP) Grant funded by the MSIT (Augmented Beam-Routing: Carom-MIMO) under Grant 2021-0-00486. The associate editor coordinating the review of this article and approving it for publication was Y. Mao. *(Corresponding authors: Bang Chul Jung; Young Dam Kim.)*

Young-Seok Lee and Bang Chul Jung are with the Department of Electrical and Computer Engineering, Ajou University, Suwon 16499, South Korea (e-mail: wiclyslee@gmail.com; bcjung@ajou.ac.kr).

Young Dam Kim is with the Department of Electronics Engineering, Chungnam National University, Daejeon 34134, South Korea (e-mail: youngdamkim@cnu.ac.kr).

Digital Object Identifier 10.1109/LWC.2024.3520082

[1]The discrete UCA-based OAM system was analyzed based on electromagnetic theory by considering several transmit polarizations in [13].

2162-2345 © 2024 IEEE. All rights reserved, including rights for text and data mining, and training of artificial intelligence and similar technologies. Personal use is permitted, but republication/redistribution requires IEEE permission.
See https://www.ieee.org/publications/rights/index.html for more information.
Authorized licensed use limited to: AJOU UNIVERSITY. Downloaded on March 12,2025 at 01:23:45 UTC from IEEE Xplore. Restrictions apply.

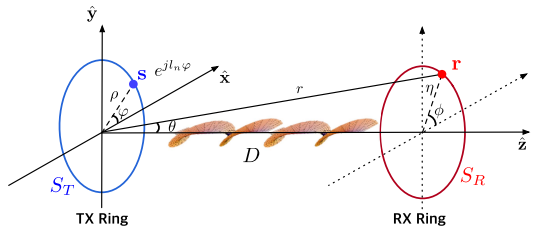

Fig. 1. System model of CAP-OAM systems with continuous ring antenna-based transceiver.

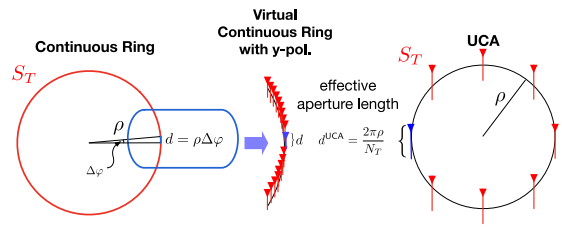

Fig. 2. Comparison of CAP-OAM system with UCA-OAM system based on current distributed region S_T.

transmit continuous ring denoted S_T can be expressed with respect to the radius of ρ and the positive angle $\varphi(\in (0, 2\pi])$ about the x-axis as

$$\mathbf{s} = \rho\cos\varphi\hat{\mathbf{x}} + \rho\sin\varphi\hat{\mathbf{y}}, \tag{1}$$

where $\hat{\mathbf{x}}$, $\hat{\mathbf{y}}$, and $\hat{\mathbf{z}}$ denote the unit vector of x, y, and z-axis, respectively. An observation point $\mathbf{r}(\in \mathbb{R}^3)$ on the receive continuous ring denoted S_R is expressed with respect to the positive angle $\phi(\in (0, 2\pi])$ about the x-axis, the elevation angle $\theta(\in [-\pi/2, \pi/2])$ about the z-axis, and the distance from origin to the $\mathbf{r}$ on the S_R, i.e., $r = \sqrt{D^2 + \eta^2}$ as follows

$$\mathbf{r} = r\sin\theta\cos\phi\hat{\mathbf{x}} + r\sin\theta\sin\phi\hat{\mathbf{y}} + r\cos\theta\hat{\mathbf{z}}. \tag{2}$$

A set of OAM modes is denoted as $\mathcal{N}(\subset \mathbb{Z})$ and the number of OAM modes is assumed to be N, i.e., $|\mathcal{N}| = N$ where $|\cdot|$ denotes the cardinality of a set. For example, if $\mathcal{N} = \{-1, 0, 1\}$, then $N = 3$. For a fair comparison between the continuous aperture antenna system and classical discrete antenna systems, the transmit current distribution of the CAP-OAM system, $\mathbf{J}(\mathbf{s})(\in \mathbb{C}^3)$, should satisfy the following power constraint,

$$P_T = \int_{S_T} |\mathbf{J}(\mathbf{s})|^2 d\mathbf{s} = \sum_{n=1}^{N} \int_{S_T} |\mathbf{J}_n(\mathbf{s})x_n|^2 d\mathbf{s}, \tag{3}$$

where $\mathbf{J}_n(\mathbf{s})(\in \mathbb{C}^3)$ denotes the current distribution of the $n(\in \{1, \ldots, N\})$-th OAM mode and $x_n(\in \mathbb{C})$ denotes n-th transmit symbol. We assume the equal power allocation for each OAM mode at the transmitter, and the n-th symbol power becomes equal to P_T/N. Thus, $\mathbf{J}_n(\mathbf{s})$ is designed to be normalized over S_T. Since OAM mode generation with y-polarization among various polarizations with circular arrays is appropriate for pure OAM mode propagation [13], the n-th current distribution with power constraint (3) is designed as

$$\mathbf{J}_n(\mathbf{s}) = \frac{e^{jl_n\varphi}}{\sqrt{2\pi\rho}}\hat{\mathbf{y}}, \tag{4}$$

where $l_n(\in \mathcal{N})$ denotes the n-th OAM mode integer. As shown in (4), since the transmit current distribution for the OAM mode beam is related to the spatial angle of the transmit antenna, a continuous ring-based OAM transmitter can generate an arbitrary OAM transmit current distribution, unlike the UCA with a discrete antenna structure. In other words, as (4) is interpreted as a basis function, continuous ring-based OAM systems can be regarded as CAP-OAM systems from the point of view of CAP-MIMO or holographic MIMO.

On the other hand, the metamaterial-based antenna system utilizes the phase and amplitude discontinuity of the EM wave or mutual coupling between tiny meta-atoms spaced within half a wavelength and the interface [15]. When strictly forming (4), the scattering matrix between each active meta-atom element must be considered [16]. However, our main contribution is to investigate the ultimate performance of OAM-based communication systems with continuous-aperture transceivers as in related studies [3], [12]. Therefore, in this letter, we assume that a continuous ring antenna is modeled as a complete continuum consisting of infinite tiny antennas to derive the fundamental electromagnetic channel and performance limits of the CAP-OAM as in [1]. In other words, (4) can be assumed to have already considered mutual coupling between tiny elements, assuming the entire continuous ring as one element.

Remark 1: **[CAP-OAM vs. UCA-OAM]** The CAP-OAM system can be regarded as a generalized and asymptotic form of classical UCA-OAM systems. As shown in Fig. 2, the current distribution must be considered over the region where the source point $\mathbf{s}$ exists even in the conventional UCA transmitter. When the effective length of each (polarized) antenna element in the UCA is assumed to be d^{UCA}, the power constraint can be represented for the y-polarization as follows

$$P_T = \sum_{u=1}^{N_T}\sum_{n=1}^{N}\int_0^{d^{\mathsf{UCA}}} \left|\mathbf{J}_n^{(u)}(\mathbf{s})x_n\right|^2 d\mathbf{s}, \tag{5}$$

where N_T denotes the number of UCA elements and $\mathbf{J}_n^{(u)}(\mathbf{s})(\in \mathbb{C}^3)$ denotes the n-th current distribution of the $u(\in \{1, \ldots, N_T\})$-th element of UCA antenna, which is defined as

$$\mathbf{J}_n^{(u)}(\mathbf{s}) = \frac{e^{jl_n\varphi_u}}{\sqrt{N_T d^{\mathsf{UCA}}}}\hat{\mathbf{y}}. \tag{6}$$

Assuming a single UCA antenna element with a length of $d^{\mathsf{UCA}} = 2\pi\rho/N_T$ as in [13], we model the current distribution of the UCA-OAM system. With this setup, the effective aperture length of the UCA-OAM system, which is the summation of lengths of all dipole antenna elements, becomes $2\pi\rho$. It is worth noting that if both systems have the same size of physical antenna aperture, the CAP-OAM system can be interpreted as the generalized and asymptotic form of the classical UCA-OAM system without mutual coupling. We analyze and compare both systems through a unified analytical framework.

III. Channel Modeling of CAP-OAM Systems: From Continuous Channel to Discrete Channel

Using the current distribution and definition of dyadic Green's function, the electric field $\mathbf{E}(\mathbf{r})(\in \mathbb{C}^3)$ is given by

$$\mathbf{E}(\mathbf{r}) = \int_{S_T} \mathbf{G}(\mathbf{r}, \mathbf{s})\mathbf{J}(\mathbf{s})\ d\mathbf{s}, \tag{7}$$

Authorized licensed use limited to: AJOU UNIVERSITY. Downloaded on March 12,2025 at 01:23:45 UTC from IEEE Xplore. Restrictions apply.

where dyadic Green's function $\mathbf{G}(\mathbf{r},\mathbf{s})(\in \mathbb{C}^{3\times 3})$ is defined as

$$\begin{aligned}\mathbf{G}(\mathbf{r},\mathbf{s}) &= jkZ_0\left\{\mathbf{I}+\frac{1}{k^2}\nabla\nabla^T\right\}\frac{e^{jk\|\mathbf{r}-\mathbf{s}\|}}{4\pi\|\mathbf{r}-\mathbf{s}\|},\\ &\overset{(a)}{\approx} jkZ_0\frac{e^{jk\|\mathbf{r}-\mathbf{s}\|}}{4\pi\|\mathbf{r}-\mathbf{s}\|}\left(\mathbf{I}-\hat{\mathbf{p}}\hat{\mathbf{p}}^T\right),\end{aligned} \tag{8}$$

where k denotes wavenumber, Z_0 denotes intrinsic impedance ($\approx 377\Omega$), $\nabla \triangleq [\frac{\partial}{\partial x},\frac{\partial}{\partial y},\frac{\partial}{\partial z}]^T$ indicates del operator, and $\hat{\mathbf{p}}=\mathbf{r}-\mathbf{s}/\|\mathbf{r}-\mathbf{s}\|$. Here, (a) represents an approximation of the dyadic Green's function using Taylor series expansion [17]. The term $\|\mathbf{r}-\mathbf{s}\|$ in the denominator of (8) can be approximated by r, but the exponent cannot be approximated that way since it is the ratio of $\|\mathbf{r}-\mathbf{s}\|$ to wavelength. Hence, assuming that the transmission distance is greater than the radius of the transmit continuous ring, i.e., $r \gg \rho$ [3], the distance between an observation point and a source point can be approximated as

$$\|\mathbf{r}-\mathbf{s}\| \approx r-\rho\sin\theta\cos(\phi-\varphi). \tag{9}$$

Similarly, through the same assumption, $r \gg \rho$, $\hat{\mathbf{p}}\hat{\mathbf{p}}^T$ can also be approximated as

$$\hat{\mathbf{p}}\hat{\mathbf{p}}^T \approx \begin{bmatrix}\sin^2\theta\cos^2\phi & \sin^2\theta\cos\phi\sin\phi & \sin\theta\cos\theta\cos\phi\\ \sin^2\theta\cos\phi\sin\phi & \sin^2\theta\sin^2\phi & \sin\theta\cos\theta\sin\phi\\ \sin\theta\cos\theta\cos\phi & \sin\theta\cos\theta\sin\phi & \cos^2\theta\end{bmatrix}. \tag{10}$$

By applying (4) and (8)-(10) to (7), the electric field of CAP-OAM is derived as (11) at the bottom of the page.
In (11), $J_{l_n}(\cdot)$ denotes the Bessel function of the first kind for integer order l_n. We can observe that when the l_n OAM mode propagates, not only the pure l_n mode but also several inter-mode interference signals occur in (11). For example, the l_n+2 and l_n-2 modes emerge for both x- and y-polarizations, and the l_n+1 and l_n-1 modes for z-polarization. In particular, it can be seen from (11) that right-hand circular polarization (RHCP) and left-hand circular polarization (LHCP) are generated for l_n+2 mode and l_n-2 mode, respectively. As a result, the l_n-mode OAM propagated with y-polarized wave has a pure l_n-mode OAM propagation component only in the y-polarization.

In order to retrieve pure OAM modes included in the y-polarization, the $m(\in\{1,\ldots,N\})$-th receive current distribution $\mathbf{\Psi}_m(\mathbf{r})(\in\mathbb{C}^3)$ of the CAP-OAM is designed as

$$\mathbf{\Psi}_m(\mathbf{r}) = \frac{e^{jl_m\phi}}{\sqrt{2\pi\eta}}\,\hat{\mathbf{y}}, \tag{12}$$

where $l_m(\in\mathcal{N})$ denotes the m-th receive OAM mode. Then, by matched-filtering the m-th receive current distribution into (11) for effectively receiving the entire OAM waves arriving at the receive continuous ring, the received signal of the m-th OAM mode $y_m(\in\mathbb{C})$ is given by

$$y_m = \int_{S_R}\mathbf{\Psi}_m^H(\mathbf{r})\mathbf{E}(\mathbf{r})\,d\mathbf{r}+w_m, \tag{13}$$

where $w_m(\in\mathbb{C})$ represents the noise component when receiving the m-th OAM mode, and it is assumed to follow identical and independently distributed complex Gaussian distribution with zero-mean and variance of σ^2.

Finally, we derive an equivalent discrete channel coefficient, called the coupling coefficient, for the CAP-OAM-MDM system. Using (4) and (7), (13) can be expressed as follows

$$y_m = \sum_{n=1}^{N}\int_{S_R}\int_{S_T}\mathbf{\Psi}_m^H(\mathbf{r})\mathbf{G}(\mathbf{r},\mathbf{s})\mathbf{J}_n(\mathbf{s})\,d\mathbf{s}\,d\mathbf{r}\,x_n+w_m. \tag{14}$$

We define an equivalent discrete channel matrix $\mathbf{H}(\in\mathbb{C}^{N\times N})$ where the element H_{mn} denotes the equivalent channel coefficient from the n-th transmit OAM mode to the m-th receive OAM mode as follows

$$H_{mn} \triangleq \int_{S_R}\int_{S_T}\mathbf{\Psi}_m^H\mathbf{G}(\mathbf{r},\mathbf{s})\mathbf{J}_n(\mathbf{s})\,d\mathbf{s}\,d\mathbf{r}. \tag{15}$$

In terms of the OAM mode, if (14) is expressed as a received signal vector $\mathbf{y}(\in\mathbb{C}^N)$, a channel matrix $\mathbf{H}$, a transmitted symbol vector $\mathbf{x}(\in\mathbb{C}^N)$, and a noise vector $\mathbf{w}(\in\mathbb{C}^N)$, then it can be equivalently regarded as the received signal of the classical MIMO channels, i.e.,

$$\mathbf{y}=\mathbf{H}\mathbf{x}+\mathbf{w}. \tag{16}$$

The most important part in *information theory* is to set up the mathematical model of the channel effect between communication nodes. We will exploit (15) and (16) as the channel model of the CAP-OAM-MDM system to investigate its (information-theoretic) achievable rate performance.

By applying (11) and (12), (15) can be derived as a closed-form in (17) at the bottom of the page.
In (17), $r=\sqrt{D^2+\eta^2}$ and $\theta=\tan^{-1}\frac{\eta}{D}$ were considered. From (17), it is worth noting that the channel matrix of CAP-OAM-MDM systems does not form a unitary(or orthogonal) matrix due to the effect of circular polarization (CP) in the y-polarization as noted in (11). In other words, additional digital signal processing like singular value decomposition (SVD) to resolve inter-mode interference might be needed at the receiver of CAP-OAM-MDM systems. However, interfering channels due to CP do not significantly affect the desired channel since the ratio between channel coefficients always satisfies the following condition for a perfectly aligned transceiver:

$$\frac{2\left(1+\cos^2\left(\tan^{-1}\frac{\eta}{D}\right)\right)}{\sin^2\left(\tan^{-1}\frac{\eta}{D}\right)} > 1. \tag{18}$$

From (18), it is confirmed that the desired channel always yields the largest gain, and the channel matrix becomes a quasi-orthogonal matrix since interference channel gains converge to zero as the transmission distance increases. In the case of two perfectly aligned continuous ring antennas, the effect of CP is almost negligible.

$$\begin{aligned}\mathbf{E}(\mathbf{r}) = \sum_{n=1}^{N} kZ_0\sqrt{2\pi\rho}(-j)^{l_n}\frac{e^{jkr}}{16\pi r}J_{l_n}(k\rho\sin\theta)x_n\Big\{&(\cos^2\theta-1)e^{j(l_n+2)\phi}\left(\hat{\mathbf{x}}-e^{j\frac{\pi}{2}}\hat{\mathbf{y}}\right)+(1-\cos^2\theta)e^{j(l_n-2)\phi}\left(\hat{\mathbf{x}}+e^{j\frac{\pi}{2}}\hat{\mathbf{y}}\right)\\ &+2j\left(1+\cos^2\theta\right)e^{jl_n\phi}\hat{\mathbf{y}}-2\sin\theta\cos\theta\left(e^{j(l_n+1)\phi}-e^{j(l_n-1)\phi}\right)\hat{\mathbf{z}}\Big\}.\end{aligned} \tag{11}$$

Authorized licensed use limited to: AJOU UNIVERSITY. Downloaded on March 12,2025 at 01:23:45 UTC from IEEE Xplore. Restrictions apply.

In addition, we can observe other effects of various parameters on the closed-form equivalent discrete CAP-OAM-MDM channel in (17). For example, the radii of the transmit and receive continuous ring antenna are regarded as the array gain. The transmit OAM mode determines the order of the Bessel function of the first kind. With well-known properties of the Bessel function of the first kind, the channel coefficient diminishes as the distance from the center of the receive ring antenna increases, called beam-divergence characteristics. This tendency accelerates with increasing OAM modes and center frequency (wavenumber) as in (17). In other words, not only the OAM mode but also the transmit/receive antenna size, transmission distance, and carrier frequency determine the beam-divergence of OAM radio waves. In short, the closed-form equivalent discrete channel matrix includes various communication-theoretic parameters of CAP-OAM-MDM systems, and the resultant practical insight into these parameters can be intuitively grasped. In addition, by using each element in (17) for constructing the discrete OAM channel matrix in (16), we can also derive a closed-form of the achievable rate of CAP-OAM systems as

$$R = \log_2\left\{\det\left(\mathbf{I}_N + \frac{G_t G_r \gamma}{N}\mathbf{H}\mathbf{H}^{\mathrm{H}}\right)\right\}, \tag{19}$$

where det(·) denotes the determinant operator of a matrix, γ denotes the transmit SNR, i.e., $\gamma = P_T/\sigma^2$, and the terms G_t and G_r represent the transmit and receive antenna gains, respectively.

IV. Degrees of Freedom of CAP-OAM Systems

Defining the effective DoF of CAP-OAM systems as in [18] is necessary for practical OAM-based communication systems. In Section III, we observe that the equivalent discrete channel matrix of CAP-OAM systems reflects many communication parameters. Hence, by exploiting the well-known SVD as in the conventional MIMO, we formally define the effective DoF of CAP-OAM systems as the number of OAM eigenmodes in which the received SNR is larger than a certain threshold as follows

$$N_{\mathsf{DoF}}(\gamma_{\mathrm{th}}) \triangleq \left|\left\{i | \gamma_{\mathrm{RX}}^i \geq \gamma_{\mathrm{th}}, 1 \leq i \leq N\right\}\right|, \tag{20}$$

and the received SNR γ_{RX}^i for $i(\in\{1, 2, \ldots, N\})$-th largest OAM eigenmode is defined as

$$\gamma_{\mathrm{RX}}^i = \frac{G_t G_r \sigma_i^2}{N}\gamma, \quad i \in \{1, 2, \ldots, N\}, \tag{21}$$

where σ_i means the i-th singular value of $\mathbf{H}$. The threshold γ_{th} can be adjusted according to system requirements or usages of the effective DoF. For example, the effective DoF can be used to approximate the achievable rate of the CAP-OAM system:

$$R \approx \sum_{i=1}^{N_{\mathsf{DoF}}} \log_2\left(1 + \gamma_{\mathrm{RX}}^i\right). \tag{22}$$

TABLE I
Simulation Parameters

Parameter	Value
Carrier frequency (f)	100GHz
Radius of TX ring (ρ)	$100\lambda(\approx 30\mathrm{cm})$
Radius of RX ring (η)	$200\lambda(\approx 60\mathrm{cm})$
Transmit OAM mode set ($\mathcal{N}$)	$\{-10, \cdots, -1, 0, 1, \cdots, 10\}$
No. of OAM modes (N)	21
Transmit SNR per mode (γ/N)	40dB
TX & RX Antenna Gain (G_t, G_r)	1
The received SNR threshold (γ_{th})	0dB

V. Simulation Results

For validating CAP-OAM systems, we assume the complete continuum consisting of many tiny antennas for emulating continuous aperture as in [1], [2], where small antenna elements are assumed to be very closely attached in the transmit/receive ring aperture. This spatially-discretized CAP-OAM system is regarded as the virtual continuous ring with y-polarization of Fig. 2. We set the effective length as $d = 0.3$mm and 0.6 mm for transmit and receive rings, respectively, which implies that both rings are modeled with 6, 284 virtual antennas. Then, we can form a continuous phase for OAM mode generation so that the overall effective length of the virtual antennas approximates the circumference of the continuous ring. Consequently, virtual antennas are used as a simulation methodology. Assuming a CAP-OAM system to be utilized for wireless backhaul, the transmit SNR for each OAM is equal to 40dB for both CAP-OAM and UCA-OAM systems [19]. The effective length of UCA antennas (d^{UCA}) is assumed to be equal to d of the CAP-OAM system since the UCA-OAM system can be considered as a sampling version of the CAP-OAM system when mutual coupling is not considered. The number of antennas at the transmitter and receiver is assumed to be the same in the UCA-OAM system. Simulation parameters are summarized in Table I.

First, we examine whether the CAP-OAM system effectively generates pure OAM modes by investigating the amplitude and phase distributions of the electric field. Fig. 3 compares amplitude and phase distributions of OAM waves with the 8-element UCA-OAM system and the CAP-OAM system for several OAM modes. Here, the electric field of the UCA-OAM system was calculated numerically based on [13]. In Fig. 3, the received electric fields are observed on a square surface with a length of 2 meters. The transmission distance is set to 75 meters, which forms the near-field radio communication channel if we consider the center frequency. It is observed that the CAP-OAM system better generates pure OAM waves

$$H_{mn} = \begin{cases} 2\pi\sqrt{\rho\eta}kZ_0(-j)^{l_n}\frac{e^{jk\sqrt{D^2+\eta^2}}}{16\pi\sqrt{D^2+\eta^2}}J_{l_n}\left(k\rho\sin\left(\tan^{-1}\frac{\eta}{D}\right)\right)j2\left(1+\cos^2\left(\tan^{-1}\frac{\eta}{D}\right)\right), & l_m = l_n, \\ 2\pi\sqrt{\rho\eta}kZ_0(-j)^{l_n}\frac{e^{jk\sqrt{D^2+\eta^2}}}{16\pi\sqrt{D^2+\eta^2}}J_{l_n}\left(k\rho\sin\left(\tan^{-1}\frac{\eta}{D}\right)\right)j\sin^2\left(\tan^{-1}\frac{\eta}{D}\right), & l_m = l_n \pm 2, \\ 0, & \text{otherwise}. \end{cases} \tag{17}$$

Authorized licensed use limited to: AJOU UNIVERSITY. Downloaded on March 12,2025 at 01:23:45 UTC from IEEE Xplore. Restrictions apply.

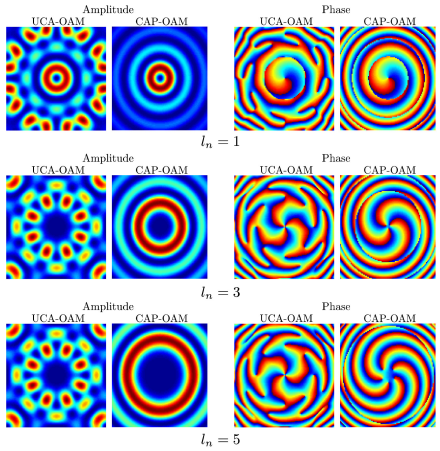

Fig. 3. Amplitude (left two figures) and phase (right two figures) distributions of electric-field of several OAM modes generated by both UCA-OAM and CAP-OAM systems.

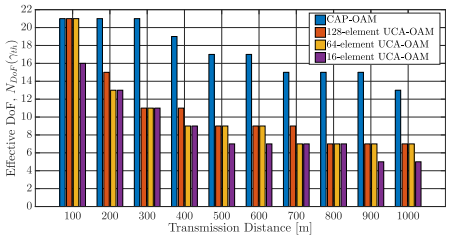

Fig. 4. Effective DoF of CAP-OAM system as a function of transmission distance D when $\gamma_{\mathrm{th}} = 0\mathrm{dB}$.

than the UCA-OAM system for all OAM modes. Moreover, $l_n = 5$ OAM mode cannot be generated by the conventional 8-element UCA antennas due to the fundamental limitation of discrete antenna elements. In contrast, the CAP-OAM system generates high purity $l_n = 5$ OAM mode. High-order OAM beams diverge more for both antenna systems.

Figs. 4 and 5 compare the CAP-OAM and UCA-OAM systems regarding effective DoF and achievable rate, respectively. We set $\gamma_{\mathrm{th}} = 0\mathrm{dB}$ as a minimum received SNR for practical communication environments [20].[2] As shown in Fig. 4, the effective DoF of the CAP-OAM system is the same or larger than that of the conventional UCA-OAM system. In particular, the CAP-OAM system yields much higher effective DoF than the UCA-OAM system as transmission distance increases, even though the effective DoF of the UCA-OAM system increases as the number of antennas of the UCA-OAM increases. Interestingly, when the transmission distance is 100m, the CAP-OAM system achieves 23.92% improved achievable rate performance compared with the 128-element UCA-OAM system, and when the transmission distance is 1000m, the performance of the CAP-OAM yields a better achievable rate by 34.61%. This shows that the CAP-OAM system performs better in long-distance communication environments. In addition, as shown in Fig. 5, the achievable rate analysis with the effective DoF well estimates or approximates the actual performance since the effective DoF implies that the

[2]In practice, the threshold for elaborating the effective DoF is a design parameter that can be determined according to various system aspects for given communication environments.

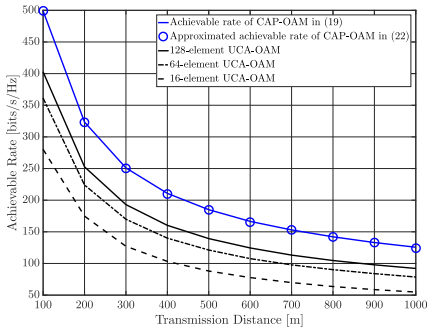

Fig. 5. Achievable rate of CAP-OAM system as a function of transmission distance D.

number of eigenmode beams affects performance significantly in practical communication environments.

References

[1] N. Decarli and D. Dardari, "Communication modes with large intelligent surfaces in the near field," *IEEE Access*, vol. 9, pp. 165648–165666, 2021.

[2] Z. Zhang and L. Dai, "Pattern-division multiplexing for continuous-aperture MIMO," in *Proc. IEEE Int. Conf. Commun.*, May 2022, pp. 3287–3292.

[3] L. Sanguinetti et al., "Wavenumber-division multiplexing in line-of-sight holographic MIMO communications," *IEEE Trans. Wireless Commun.*, vol. 22, no. 4, pp. 2186–2201, Apr. 2023.

[4] Z. Wan et al., "Mutual information for electromagnetic information theory based random fields," *IEEE Trans. Commun.*, vol. 71, no. 4, pp. 1982–1996, Apr. 2023.

[5] J. Zhu et al., "Electromagnetic information theory: Fundamentals, modeling, applications, and open problems," *IEEE Wireless Commun.*, vol. 31, no. 3, pp. 156–162, Jun. 2024.

[6] W. Cheng et al., "Orbital angular momentum for wireless communications," *IEEE Wireless Commun.*, vol. 26, no. 1, pp. 100–107, Feb. 2019.

[7] R. Chen et al., "Multi-mode OAM radio waves: Generation, angle of arrival estimation and reception with UCAs," *IEEE Trans. Wireless Commun.*, vol. 19, no. 10, pp. 6932–6947, Oct. 2020.

[8] H. Yang et al., "A THz-OAM wireless communication system based on transmissive metasurface," *IEEE Trans. Antennas Propag.*, vol. 71, no. 5, pp. 4194–4203, May 2023.

[9] W. Du et al., "A UCA-based multimodal OAM wireless backhaul model," *IEEE Commun. Lett.*, vol. 28, no. 1, pp. 24–28, Jan. 2024.

[10] M. V. Rao et al., "Generation of dual-band OAM beam using planar uniform circular array for vehicular communications," *Microw. Opt. Technol. Lett.*, vol. 66, no. 1, 2024, Art. no. e13717.

[11] W.-X. Long et al., "Low-overhead iterative channel parameter estimation for multi-user OAM wireless backhaul," *IEEE Trans. Broadcast.*, early access, Aug. 1, 2024, doi: 10.1109/TBC.2024.3434676.

[12] G. Torcolacci et al., "Holographic MIMO communications exploiting the orbital angular momentum," *IEEE Open J. Commun. Soc.*, vol. 4, pp. 1452–1469, 2023.

[13] D. Liu et al., "Theoretical analysis and comparison of OAM waves generated by three kinds of antenna array," *Digit. Commun. Netw.*, vol. 7, no. 1, pp. 16–28, 2021.

[14] W. Son et al., "Optimal design of full-duplex orbital angular momentum mode-division multiplexing systems," in *Proc. IEEE Int. Conf. Commun. Workshops*, May 2022, pp. 180–185.

[15] T. Gong et al., "Holographic MIMO communications: Theoretical foundations, enabling technologies, and future directions," *IEEE Commun. Surveys Tuts.*, vol. 26, no. 1, pp. 196–257, 1st Quart., 2024.

[16] D. M. Pozar, "The active element pattern," *IEEE Trans. Antennas Propag.*, vol. 42, no. 8, pp. 1176–1178, Aug. 1994.

[17] A. S. Y. Poon et al., "Degrees of freedom in multiple-antenna channels: A signal space approach," *IEEE Trans. Inf. Theory*, vol. 51, no. 2, pp. 523–536, Feb. 2005.

[18] A. Sawant et al., "Ultimate capacity analysis of orbital angular momentum channels," *IEEE Wireless Commun.*, vol. 28, no. 1, pp. 90–96, Feb. 2021.

[19] A. A. Amin and S. Y. Shin, "Capacity analysis of cooperative NOMA-OAM-MIMO based full-duplex relaying for 6G," *IEEE Wireless Commun. Lett.*, vol. 10, no. 7, pp. 1395–1399, Jul. 2021.

[20] K. Rikkinen et al., "THz radio communication: Link budget analysis toward 6G," *IEEE Commun. Mag.*, vol. 58, no. 11, pp. 22–27, Nov. 2020.

Authorized licensed use limited to: AJOU UNIVERSITY. Downloaded on March 12,2025 at 01:23:45 UTC from IEEE Xplore. Restrictions apply.